Available online at www.sciencedirect.com
ScienceDirect
Journal of Power Sources 172 (2007) 775–781
JOURNAL OF POWER SOURCES
www.elsevier.com/locate/jpowsour

A low-Cr metallic interconnect for intermediate-temperature solid oxide fuel cells

Shujiang Geng [a], Jiahong Zhu [a,*], Michael P. Brady [b], Harlan U. Anderson [c], Xiao-Dong Zhou [d], Zhenguo Yang [d]

[a] *Department of Mechanical Engineering, Tennessee Technological University, Cookeville, TN 38505, USA*
[b] *Oak Ridge National Laboratory, Oak Ridge, TN 37831-6115, USA*
[c] *Electronic Materials Applied Research Center, University of Missouri-Rolla, Rolla, MO 65409, USA*
[d] *Pacific Northwest National Laboratory, Richland, WA 99352, USA*

Received 23 March 2007; accepted 11 May 2007
Available online 18 May 2007

Abstract

A new low thermal expansion, low-Cr, Fe–Co–Ni base alloy was developed and evaluated as interconnect for intermediate-temperature solid oxide fuel cells (SOFCs). This alloy demonstrated good oxidation resistance, low oxide scale area specific resistance and a reasonable match in coefficient of thermal expansion with adjacent cell components. A double-layer oxide structure with an highly conductive, Cr-free $(Fe,Co,Ni)_3O_4$ spinel outer layer and a thin protective Cr_2O_3 inner layer was formed on the alloy surface upon thermal exposure in air at 800 °C. The existence of the Cr-free $(Fe,Co,Ni)_3O_4$ outer layer effectively reduced the Cr evaporation and in transpiration testing resulted in a six-fold decrease in Cr evaporation as compared to a state-of-the-art ferritic interconnect alloy. The new low-Cr alloy also exhibited good scale spallation resistance and adequate compatibility with the cathode material $La_{0.8}Sr_{0.2}MnO_3$ (LSM).

Keywords: Solid oxide fuel cell; Interconnect alloy; Oxidation resistance; Spinel; Cr volatility; Area specific resistance

1. Introduction

Solid oxide fuel cells (SOFCs) have attracted significant attention due to the potential for environmentally friendly power generation with high efficiency and fuel flexibility. However, the main hurdles thwarting the commercial introduction of SOFCs are the stack cost and durability, particularly related to the long-term stability of stack/cell materials, such as interconnect, which serves to connect individual cells in a stack to achieve useful levels of power [1–3]. The interconnect is in contact with the anode of one cell and the cathode of the next [4] and therefore must be gas tight, electrically conductive, stable in both oxidizing (cathode-side) and reducing (anode-side) environments and matching in coefficient of thermal expansion (CTE) with other cell components. Recent progress in reducing the SOFC operation temperature from 1000 °C to an intermediate temperature (IT) of about 600–800 °C allows the use of oxidation/corrosion-resistant metallic alloys as interconnects to supplant their ceramic counterpart, such as $LaCrO_3$-based perovskites [2]. Compared to a $LaCrO_3$-based interconnect, metallic alloys have a number of advantages, such as lower raw material/manufacture cost, higher thermal and electronic conductivity, significantly better mechanical properties, etc. However, the specific operating conditions of SOFC impose challenging oxidation/corrosion resistance requirements while maintaining electrical conductivity. Above about 600 °C, Al_2O_3, SiO_2 or Cr_2O_3 are the only oxides that exhibit sufficiently low growth rates to be feasible to protect heat resistant alloys for long-term use. Al_2O_3 and SiO_2 are too electrically insulating to be used for metallic interconnect alloys. NiO has also been considered [5] but has too high a CTE compared to the ceramic materials currently used for the solid electrolyte, anode and cathode components to be viable for conventional SOFC designs.

Interconnect alloy development worldwide has focused on ferritic Cr_2O_3-forming alloys for IT-SOFCs [6–8], as

* Corresponding author. Tel.: +1 931 372 3186; fax: +1 931 372 6340.
E-mail address: jzhu@tntech.edu (J. Zhu).

0378-7753/$ – see front matter © 2007 Elsevier B.V. All rights reserved.
doi:10.1016/j.jpowsour.2007.05.022

the Cr_2O_3 scale has an attractive balance of relatively low growth rate and reasonable electronic conductivity. Unfortunately, evaporation of chromia (especially in the presence of water vapor) and subsequent Cr migration in the cell and deposition at the cathode–electrolyte interface significantly degrades SOFC performance [9–11]. The amount of Cr vaporization can be reduced by applying a Cr-retaining coating to the surface of the alloys [12–15]. These coatings may help mitigate chromium volatility, reduce the oxide scale growth rate of the chromia-forming alloys on the cathode side and lower the contact or interfacial resistance between the interconnect and cathode; however, Cr outward migration via either cracks or open porosity in these coatings may still lead to degradation in SOFC performance over time. Furthermore, there are some challenges associated with coatings, including cost and reliability (especially during thermal cycling).

An alternative approach is to develop new metallic alloys capable of forming desired oxide scale structures on the alloy surface during SOFC operation to block the Cr evaporation. A ferritic alloy, Crofer 22 APU, based on the Fe–Cr–Mn–Ti–La system with about 22 wt.% Cr, has recently been developed and commercialized for IT-SOFC interconnect application [16,17]. This family of alloys represents the state-of-the-art for metallic interconnects. With the addition of a small amount of Mn, a double-layer oxide scale structure with an external $(Mn,Cr)_3O_4$ spinel layer over a Cr_2O_3 inner layer is formed upon thermal exposure. Since the spinel phase contains a lower amount of Cr than Cr_2O_3 and has a lower Cr activity, Cr evaporation is reduced compared to the conventional, ferritic Cr_2O_3-forming alloys such as Ebrite (Fe–26Cr–1Mo), but still poses a major challenge for this interconnect alloy, especially over long-term stack operation. From the interconnect alloy design point of view, the formation of a Cr-free, electrically conductive, dense and/or gas-tight outer layer is needed.

In this paper, a low-Cr Fe–Co–Ni base alloy, with a composition (in wt.%) of 30Co, 25Ni, 6Cr, 5Nb, 1.5Si, 0.1Y and Fe balance, is designed and evaluated for IT-SOFC interconnects. The Fe–Co–Ni system is selected based on its potential low CTE due to the Invar effect [18,19]. While previous work mainly focused on high-Cr ferritic alloys containing at least 16 wt.% Cr in order to develop a protective scale of chromia on the alloy surface [16,17,20], this new Fe–Co–Ni base alloy contains just 6 wt.% Cr, which is lower than that in the ferritic interconnect alloys and not high enough to initially form an external chromia scale upon thermal exposure. Instead, a Cr-free spinel outer layer is developed, which acts as a surface seal to block the Cr evaporation. A small amount of Si is added to enhance the oxidation resistance of the low-Cr alloy by promoting the formation of a protective chromia inner-layer [21]. Nb is beneficial for lowering the CTE of this new alloy. This new low-Cr Fe–Co–Ni base alloy is expected to solve the problem of Cr poisoning of the cathode via formation of a Cr-free spinel outer layer atop a protective chromia inner layer on the cathode side of SOFC.

2. Experimental

2.1. Specimen preparation

The new alloy was prepared by arc-melting and drop-casting in a chilled copper mold, starting with high-purity elements. A 80 g ingot was remelted six times to ensure compositional homogeneity. After casting, the top parts were cut off and the remaining rectangular pieces with a dimension of 12 mm × 12 mm × 50 mm were given a homogenization treatment at 1100 °C in vacuum (about 10^{-4} Pa) for 10 h, followed by furnace cooling. Oxidation and thermal expansion specimens were cut from the ingots. For the Cr transpiration experiment, larger ingots (500 g) were prepared and hot rolled to 1.5 mm strips; these strips were ground to 600-grit and cleaned with a final thickness of 1 mm.

2.2. Oxidation testing

Rectangular samples of ~10 mm × 10 mm × 1 mm with a 1 mm-diameter hole were ground to 800 grit SiC, ultrasonically cleaned in acetone and then dried for oxidation test. For isothermal oxidation, the samples were hung in alumina crucibles in a box furnace, oxidized at 800 °C in air for 12 weeks. The weight of each sample was measured immediately after furnace cooling to room temperature following each 1-week exposure. X-ray diffraction (XRD) was used to identify the phase structure of the oxide scale formed on this alloy. Polished cross-sectional samples were examined by electron probe microanalysis (EPMA) to determine the elemental distributions in the oxide scale.

Cyclic oxidation testing was also conducted to evaluate the oxide scale spallation resistance of the low-Cr alloy. A binary alloy, Fe–50Ni, was also included for comparison. Each cycle consisted of holding at 800 °C for 25 h, followed by taking the samples out of the furnace directly and cooling to room temperature in air.

2.3. Scale area specific resistance

Electrical resistance of the oxidized samples was measured using the 2-probe 4-point method from 500 to 800 °C [13,22]. For electrical resistance measurement, two of the oxidized surfaces were covered with Pt paste, and Pt meshes attached with four Pt leads were placed on top of the pastes for current collection. A constant current of 10 mA was applied across two Pt leads using a power source; the corresponding voltage drop across the other two Pt leads was then measured using a multimeter. A widely accepted parameter for scaling the electrical resistance of the oxide scales, area specific resistance (ASR) was adapted here, which reflected both the electrical conductivity and the thickness of the oxide scale.

2.4. Cr transport measurement

Cr transport experiments for the new alloy was conducted in a tube furnace at 800 °C on the alloy sheets exposed to a flowing moist air with a velocity of 1.1 cm s^{-1} for 500 h. Volatilized Cr

was transported by the air stream to the cold end of the fused silica tube where it condensed on the tube surface and on collection media. The air stream was also taken through a condenser and water bubbler to assure complete Cr collection. When the experiment was complete, nitric acid rinses were used to dissolve the collected Cr-containing condensate from the tube and collection media. This rinsate was combined with the water from the bubbler and analyzed by induction-coupled plasma (ICP)-mass spectrometry to quantitatively determine the amount of Cr volatilized during the test. Cr transport rates ($kg\,m^{-2}\,s^{-1}$) were determined by dividing the total mass of Cr volatilized by the exposed surface area of the alloy samples and the total time of exposure at temperature.

2.5. Compatibility with the cathode material

For the evaluation of chemical compatibility of the new low-Cr Fe–Co–Ni alloy with the cathode material $La_{0.8}Sr_{0.2}MnO_3$ (LSM), an LSM layer of about 20–30 μm thick was screen-printed onto the polished alloy coupons to form the alloy/cathode couples. Crofer 22 APU and a Fe–50Ni alloy were also included for comparison. These couples were annealed at 900 °C in air for 300 h. The annealing temperature was selected to accelerate the interaction/interdiffusion between the alloy and the cathode. ASR measurement of these couples was conducted to obtain the overall resistance of the alloy/cathode couples after the annealing treatment. Polished cross-sectional metallographic samples were examined by EPMA to determine the distribution of various elements in the couples, with special attention paid to the alloy/cathode interface.

2.6. Thermal expansion measurement

The thermal expansion behavior of the low-Cr Fe–Co–Ni alloy was determined with a dilatometer with round bar (length, 20 mm; diameter, 5 mm). The thermal expansion measurement was carried out from 100 to 800 °C in ambient air.

3. Results and discussion

3.1. Oxidation resistance

The specific mass change of the new low-Cr alloy in air at 800 °C as a function of oxidation time is shown in Fig. 1. Data for Crofer 22 APU is included for comparison. The low-Cr alloy experienced an initially large specific mass gain, followed by a transition to slower oxidation kinetics, consistent with a transition to protective scale formation and of comparable kinetics to those observed for the Crofer 22 APU alloy. XRD patterns in Fig. 2 and EPMA results in Fig. 3 indicate that a $(Fe,Co,Ni)_3O_4$ spinel layer was developed on the low-Cr alloy during the early period of oxidation. Peaks of chromia were not observed from the XRD patterns of the thermally grown oxide scale on the low-Cr alloy after oxidation for 3 weeks at 800 °C (Fig. 2(3)); both Cr_2O_3 and $CrNbO_4$ were detected upon lightly polishing off the outer surface oxide layer and repeating the XRD measurements, as shown in Fig. 2(4). Fig. 3 indicates that

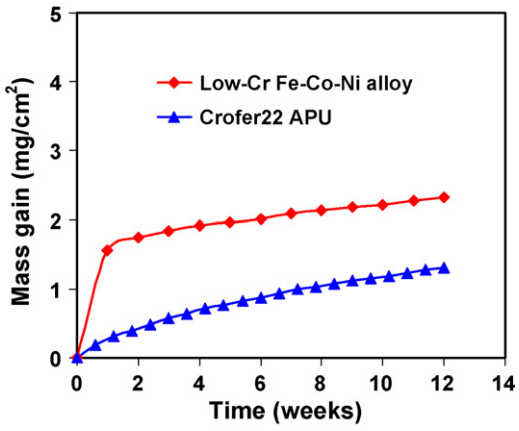

Fig. 1. Isothermal oxidation kinetics of the low-Cr Fe–Co–Ni alloy in air at 800 °C.

the spinel top layer was essentially free of Cr, and a thin Cr-rich inner oxide layer was formed at the alloy/spinel interface after a 3-week oxidation at 800 °C.

During the initial stage of oxidation, the scale consisted mainly of Fe, with some additional presence of Co and Ni, resulting in rapid weight gain and subsequent formation of the $(Fe,Co,Ni)_3O_4$ spinel layer as indicated in Figs. 1–3. Following formation of the spinel layer, Cr was enriched near the substrate adjacent to the scale as a result of the depletion of Fe, Co and Ni at that location. The oxygen partial pressure at the spinel/alloy interface was decreased due to establishment of the surface spinel layer. As a result, selective oxidation of Cr was promoted, leading to the formation of a continuous chromia inner layer

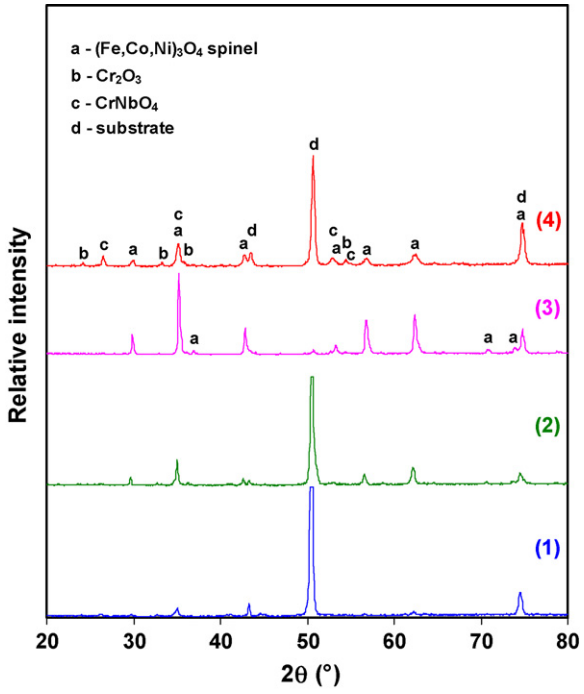

Fig. 2. XRD patterns of oxide scale formed on low-Cr Fe–Co–Ni alloy after oxidation in air at 800 °C for (1) 5 h; (2) 30 h; (3) 3 weeks (504 h), respectively, and (4) after the top oxide layer formed during 3-week exposure was partially polished off.

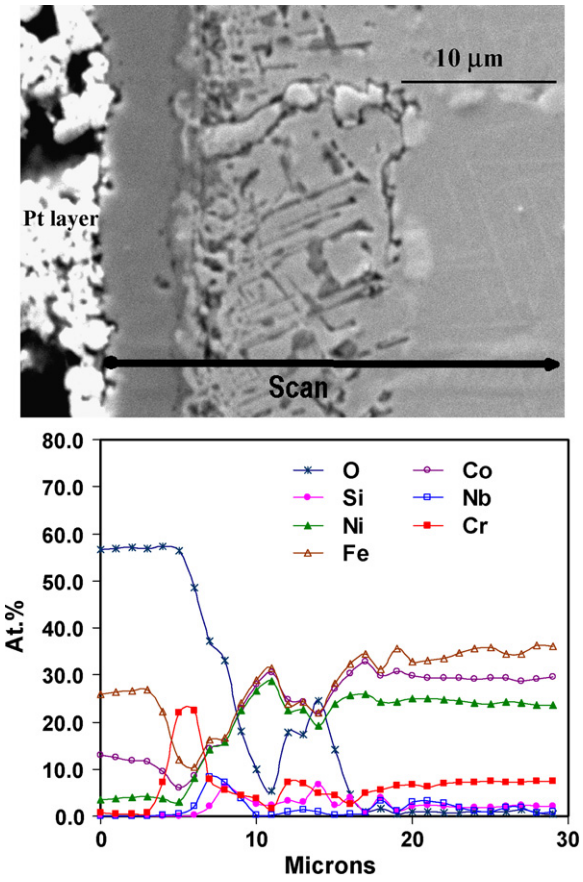

Fig. 3. EPMA results of the oxide scale formed on the low-Cr Fe–Co–Ni alloy after oxidation for 3 weeks in air at 800 °C.

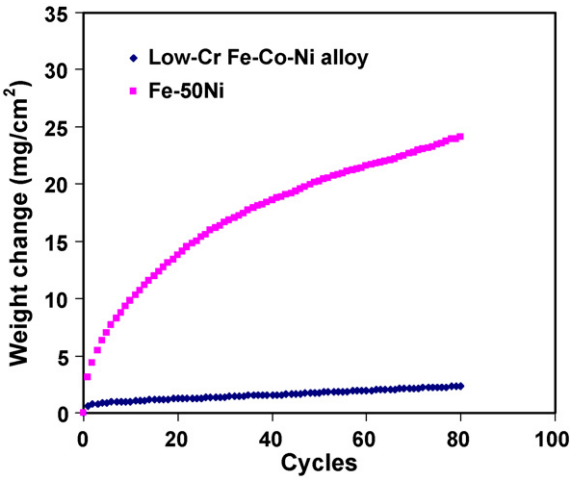

Fig. 4. Cyclic oxidation kinetics of the low-Cr Fe–Co–Ni base alloy and Fe–50Ni at 800 °C in air.

in contact with internal oxides of mainly Cr_2O_3 and $CrNbO_4$ (Figs. 2 and 3). Furthermore, the Si and Nb significantly aided the formation of the chromium oxide via a secondary oxygen getter-type effect [21,23]. This inner layer served to effectively reduce the rate of oxidation and slow down the continued growth of the outer spinel layer. Some Si enrichment in the internal oxidation zone was also evident in Fig. 3 and might also have contributed to the reduced oxidation rate; however, continuous SiO_2 layer formation was not observed by SEM/EPMA analysis, which is consistent with the ASR results shown later.

Fig. 4 shows the cyclic oxidation kinetics of the new low-Cr alloy as well as a control alloy Fe–50Ni. Continual specific mass gains were observed for both alloys; furthermore, the oxidation resistance of the low-Cr alloy was drastically improved over the Fe–50Ni alloy, consistent with the isothermal oxidation results shown in Fig. 1. After 80 cycles, no scale spallation was detected for either of the alloys. The excellent scale spallation resistance for these alloys is a result of the close match in CTE between the substrate and the surface spinel phase, which is expected to lead to low thermal stress build-up during thermal cycling for these alloys [24].

3.2. Cr volatility

The rapid formation of the Cr-free spinel outer layer prior to the establishment of the chromia inner layer is expected to effectively reduce the Cr volatile species, such as CrO_3 and $CrO_2(OH)_2$ originating from the chromia layer. This was confirmed by quantitative Cr volatility measurements for the alloy samples exposed to moist air at 800 °C for 500 h. The Cr transport rate was calculated to be 5.7×10^{-12} kg m^{-2} s^{-1} for the low-Cr alloy for an air velocity of 1.1 cm s^{-1}. For comparison under identical conditions, a value of 3.3×10^{-11} kg m^2 s^{-1} was obtained for Crofer 22 APU. Thus, the Cr volatility for the low-Cr alloy was about a factor of 6 lower than that for Crofer 22 APU which forms the $(Mn,Cr)_3O_4$ spinel overlying Cr_2O_3.

The effective reduction in Cr transport rate for the low-Cr alloy as compared to Crofer 22 APU results from the differences in the surface oxide formation sequence as well as the Cr content/activity in the surface spinel for these two alloys. For Crofer 22 APU, significant quantities of Cr are involved in the early stage of oxidation [15,25]. A Cr-containing spinel outer layer was formed and chromium vaporization from the $(Mn,Cr)_3O_4$ spinel layer was detected in spite of the relatively low thermodynamic activity of Cr in $(Mn,Cr)_3O_4$ [26], which could potentially lead to Cr migration to, and accumulation at, the cathode over long-term stack operation. Crofer 22 APU was designed to balance a number of properties, including oxidation resistance, scale ASR, formability, cost and Cr volatility. Even though a reduced Cr volatility was obtained compared to other chromia-forming alloys, this alloy was intended to be used with a Cr-blocking surface coating. For example, a Cr-free protection layer of $Mn_{1.5}Co_{1.5}O_4$ spinel was synthesized on Crofer 22 APU via slurry coating technology, which acted effectively as a barrier to outward migration of Cr and therefore resulted in a stable electrochemical performance of SOFCs [15]. However, a coating process would increase the overall cost of the interconnect material, and its long-term stability is yet to be demonstrated. For the new low-Cr alloy, the Cr-free surface spinel layer is formed *in situ* during the initial stages of oxidation, such that a coating is not necessary.

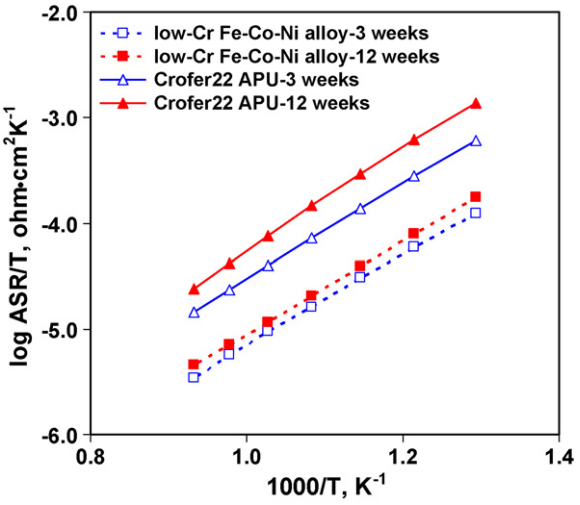

Fig. 5. Scale ASR for the low-Cr Fe–Co–Ni alloy after oxidation for 3 and 12 weeks in air at 800 °C, as compared to that for Crofer 22 APU.

3.3. Electrical property of thermally grown oxide scale

One of the key requirements for SOFC interconnect materials is a relatively low and stable scale ASR for the interconnect alloys during cell operation. The scale ASR for the new low-Cr Fe–Co–Ni alloy after oxidation for two different durations (3 and 12 weeks) in air at 800 °C was compared with that for Crofer 22 APU under the same exposure conditions. As shown in Figs. 1 and 5, even though the overall specific mass gain of the low-Cr alloy was higher (thicker oxide scale) than that of Crofer 22 APU, its scale ASR was lower than that for Crofer 22 APU. Most noticeably, the scale ASR for the low-Cr alloy after oxidation for 12 weeks was almost the same as that for 3 weeks (Fig. 5), consistent with the oxidation kinetics shown in Fig. 1 and clearly more stable than Crofer 22 APU.

This lower scale ASR for the low-Cr alloy over Crofer 22 APU is related to the different surface oxide structures formed on these two alloys. As shown in Fig. 3, the oxide scale developed on the new low-Cr alloy after oxidation at 800 °C in air consisted of a $(Fe,Co,Ni)_3O_4$ spinel outer layer and a thin chromia inner layer, whereas the oxide scale formed on Crofer 22 APU after oxidation in the same condition was comprised of a $(Mn,Cr)_3O_4$ outer layer and a relatively thick chromia-rich inner layer [17,22]. The lower scale ASR for the low-Cr alloy might be attributed to the higher electrical conductivity of $(Fe,Co,Ni)_3O_4$ compared to $(Mn,Cr)_3O_4$ and Cr_2O_3 [27,28] and/or the subsequently lower contact or interfacial resistance between $(Fe,Co,Ni)_3O_4$ and Pt (used for electrical contact in these experiments) compared to between $(Mn,Cr)_3O_4$ and Pt. Moreover, the chromia inner layer formed on the low-Cr alloy was thinner than that on Crofer 22 APU. It was also found that the scale ASR values were essentially the same prior to and after grinding/polishing of the four edges of the oxidized specimen, indicating that the electrical conduction was through the specimen thickness and not around the edges.

3.4. Compatibility with LSM

Initial testing with screen-printed couples of the new low-Cr alloy with the cathode material LSM indicates that the new alloy is compatible with the LSM cathode. After thermal exposure at 900 °C in air for 300 h, no obvious interaction or interdiffusion was observed between the LSM layer and the oxide scale formed on the low-Cr alloy; also, no Cr migration to the cathode was detected, as shown in Fig. 6. From Fig. 6(a–c), it is clear that the desired double-layer oxide scale was formed between the alloy substrate and the cathode paste. The outer oxide layer was a Cr-free spinel rich in Fe, while the inner layer was rich in Cr. The ASR of the low-Cr alloy/LSM couple was lower than that of the binary Fe–50Ni alloy/LSM or Crofer 22 APU/LSM

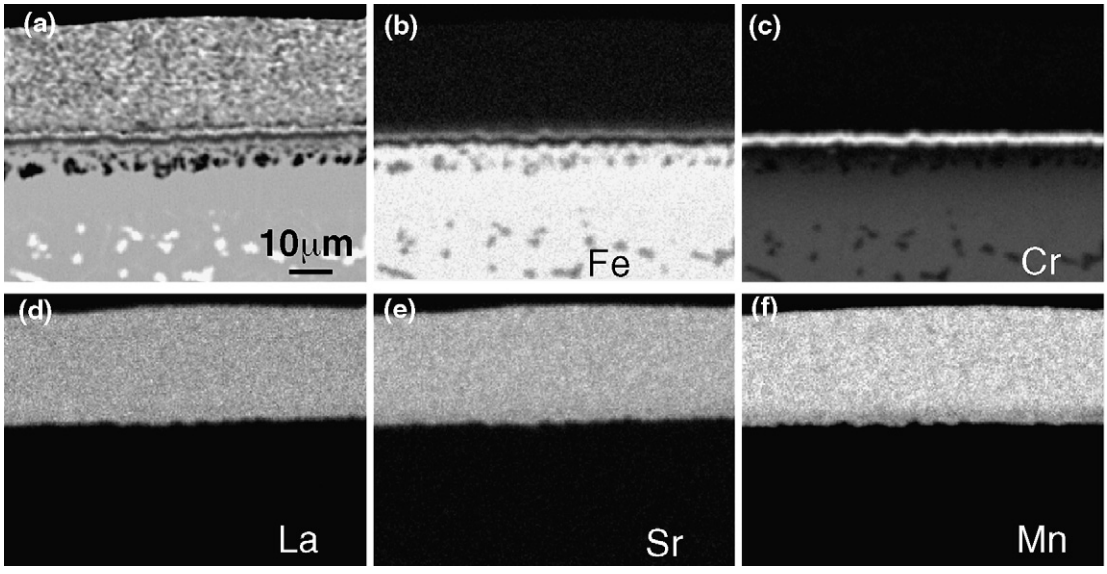

Fig. 6. Cross-section of the low-Cr Fe–Co–Ni alloy/cathode couple after oxidation for 300 h at 900 °C in air: (a) SEM image; (b) Fe mapping; (c) Cr mapping; (d) La mapping; (e) Sr mapping; (f) Mn mapping.

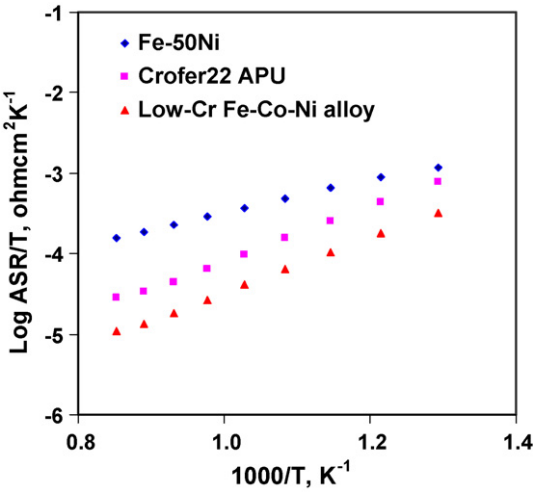

Fig. 7. ASR of the low-Cr Fe–Co–Ni alloy/LSM couple after oxidation for 300 h at 900 °C in air, as compared to that of the Fe–50Ni/LSM and Crofer 22 APU/LSM couples.

couple after similar exposure (Fig. 7), implying that no new insulating phase formed between the cathode and the low-Cr alloy. The lower ASR for the new alloy might again be attributed to the formation of a higher electrically conductive spinel layer between the cathode and the alloy substrate. The higher ASR for the Fe–50Ni/LSM couple was due to the extensive oxidation of the substrate alloy at such a high exposure temperature.

3.5. Additional discussion on the suitability of the new alloy as SOFC interconnect

Based on the above results, the new low-Cr Fe–Co–Ni base alloy is quite promising for SOFC interconnect application, especially with the potential to mitigate the Cr poisoning issues that plague the current state-of-the-art high Cr ferritic alloys. However, there are still some concerns with this new alloy that needs to be addressed, as elaborated below.

Fig. 8 shows the thermal expansion behavior of this new alloy, along with some other alloys. Although it exhibited an overall good match in thermal expansion behavior with other major cell components, such as the electrolyte, cathode and anode over the temperature range of 100–800 °C, the slope of the thermal expansion curve of the new alloy increased noticeably at temperatures above ~400 °C. The existence of such a slope change might lead to thermal stress build-up in the stacks during thermal cycling. Additional alloy design is needed to either eliminate this change or push the corresponding temperature to above 800 °C.

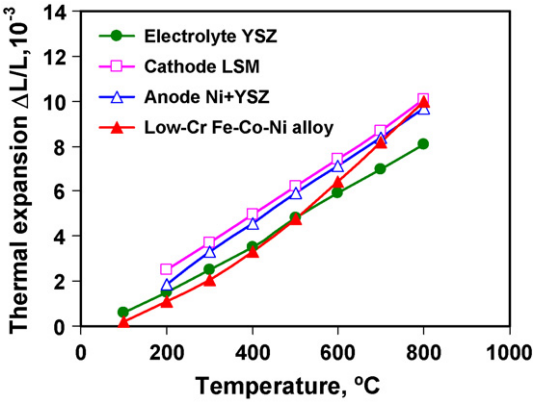

Fig. 8. Thermal expansion vs. temperature for the low-Cr Fe–Co–Ni alloy, as compared to other cell components.

The new alloy is also expected to be more expensive than current ferritic alloys, as it contains significant amounts of Co and Ni. However, the potential to be used without a coating may ultimately render these materials more cost-effective than the ferritics. Further, they could also find use as a coating or cladding material on very low-cost substrates (low-Cr steels, etc.), as the thermally grown $(Fe,Co,Ni)_3O_4$ spinel outer layer could mitigate the Cr migration and act as an electrical contact layer between the cathode and interconnect in SOFC stacks to reduce the cathode/interconnect interfacial resistance [29].

Also, while in short-term testing this alloy exhibited a good combination of oxidation resistance and oxide scale conductivity, additional work is clearly needed to examine the long-term performance of this new alloy in SOFC operation conditions.

4. Conclusions

The new low-Cr Fe–Co–Ni base alloy is a promising alternative to replace high-Cr ferritic alloys as interconnect for IT-SOFCs. A double-layer oxide scale with an electrically conductive, Cr-free $(Fe,Co,Ni)_3O_4$ spinel outer layer, which significantly blocked the Cr volatility, and a protective inner Cr_2O_3 layer, which slowed down the further oxidation process, was developed on this new alloy upon thermal exposure in air. The dual-layer oxide structure demonstrated an excellent scale spallation resistance and electrical conductivity. The new alloy also exhibited adequate compatibility with the cathode material LSM.

Acknowledgements

The authors gratefully acknowledge financial support from DOE Solid State Energy Conversion Alliance Program (DE-FC26-04NT42223) and National Science Foundation (Grant #DMR-0238113). Oak Ridge National Laboratory is managed by UT-Battelle, LLC for the US DOE under contract DE-AC05-00OR22725. The help with Cr transpiration measurement and data interpretation by Gary Maupin and Jeffry Stevenson at Pacific Northwest National Laboratory is highly appreciated.

References

[1] R.F. Service, Science 288 (2000) 1955–1957.
[2] B.C.H. Steel, A. Heinzel, Nature 414 (2001) 345–352.
[3] L. Antoni, Mater. Sci. Forum 461–464 (2004) 1073–1090.
[4] N.Q. Minh, J. Am. Ceram. Soc. 76 (3) (1993) 563–588.
[5] M.P. Brady, B.A. Pint, Z.G. Lu, J.H. Zhu, C.E. Milliken, E.D. Kreidler, L. Miller, T.R. Armstrong, L.R. Walker, Oxid. Met. 65 (3/4) (2006) 237–261.
[6] W.J. Quadakkers, J. Piron-Abellan, V. Shemet, L. Singheiser, Mater. High Temp. 20 (2) (2003) 115–127.

[7] Z. Yang, K.S. Weil, D.M. Paxton, J.W. Stevenson, J. Electrochem. Soc. 150 (9) (2003) A1188–A1201.
[8] J.W. Fergus, Mater. Sci. Eng. A 397 (2005) 271–283.
[9] S.P.S. Badwal, R. Deller, K. Foger, Y. Ramprackash, J.P. Zhang, Solid State Ionics 99 (1997) 297–310.
[10] Y. Matsuzaki, I. Yasuda, Solid State Ionics 132 (2000) 271–278.
[11] S. Taniguchi, M. Kadowaki, H. Kawamura, T. Yasuo, Y. Akiyama, Y. Miyake, T. Saitoh, J. Power Sources 55 (1995) 73–79.
[12] G. Schiler, R. Henne, R. Ruckdäschel, J. Adv. Mater. 32 (1) (2000) 3–8.
[13] J.H. Zhu, Y. Zhang, A. Basu, Z.G. Lu, M. Paranthaman, D.F. Lee, E.A. Payzant, Surf. Coat. Technol. 177 (2004) 65–72.
[14] K. Fujita, K. Ogaswara, Y. Matsuzaki, T. Sakurai, J. Power Sources 131 (2004) 261–269.
[15] Z. Yang, G.G. Xia, S.P. Simner, J.W. Stevenson, J. Electrochem. Soc. 152 (9) (2005) A1896–A1901.
[16] W.J. Quadakkers, V. Shemet, L. Singheiser, High-Temperature Material, US Patent 20,030,059,335 (2003).
[17] Z. Yang, J.S. Hardy, M.S. Walker, G.G. Xia, S.P. Simner, J.W. Stevenson, J. Electrochem. Soc. 151 (11) (2004) A1825–A1831.
[18] E.D. Wanner, D.A. DeAntonio, in: D.L. Antolovich, R.W. Stusrud, R.A. MacKay, D.L. Anton, T. Khan, R.D. Kissinger, D.L. Klarstrom (Eds.), Superalloys (Conference Proceedings), TMS, 1992, pp. 237–46.
[19] J.H. Zhu, S.J. Geng, D.A. Ballard, Int. J. Hydrogen Energy (2006), doi:10.1016/j.ijhydene.2006.08.026.
[20] T. Brylewski, M. Nanko, T. Maruyama, K. Przybylski, Solid State Ionics 143 (2) (2001) 131–150.
[21] J.M. Oh, J. Electrochem. Soc. 135 (3) (1988) 749–755.
[22] S.J. Geng, J.H. Zhu, Z.G. Lu, Solid State Ionics 177 (5–6) (2006) 559–568.
[23] L.V. Ramanathan, M. Pohl, A.F. Padiha, Mater. Corros. 46 (1995) 71–75.
[24] J.H. Zhu, S.J. Geng, Z.G. Lu, D.A. Ballard, J. Electrochem. Soc. (2007), Unpublished results.
[25] S.P. Simner, M.D. Anderson, G.G. Xia, Z. Yang, L.R. Pederson, J.W. Stevenson, J. Electrochem. Soc. 152 (4) (2005) A740–A745.
[26] C. Gindorf, L. Singheiser, K. Hilpert, Steel Res. 72 (11–12) (2001) 528–533.
[27] H. Ling, A. Petric, Electrochem. Soc. Proc., 2005–07 (2005) 1866–1873.
[28] W.Z. Zhu, S.C. Deevi, Mater. Sci. Eng. A 348 (2003) 227–243.
[29] Z.G. Yang, G.G. Xia, P. Singh, J.W. Stevenson, J. Power Sources 155 (2006) 246–252.